Journal of Molecular Liquids 454 (2026) 129573

Contents lists available at ScienceDirect

Journal of Molecular Liquids

journal homepage: www.elsevier.com/locate/molliq

Oleic acid: geraniol or cinnamyl alcohol hydrophobic mixtures: thermophysical properties and quercetin solubility

Ana Gavín [a], Daniel Juan [a], José Muñoz-Embid [a,b], Mohammadreza Haftbaradaran Esfahani [a], Carlos Lafuente [a,b], Manuela Artal [a,b,*]

[a] Departamento de Química Física, Facultad de Ciencias, Universidad de Zaragoza, Zaragoza, Spain
[b] Instituto Agroalimentario de Aragón - IA2 (Universidad de Zaragoza - CITA), Zaragoza, Spain

ARTICLE INFO

Keywords:
Hydrophobic eutectic solvents
Oleic acid
Quercetin
Thermophysical characterization
Solubility

ABSTRACT

The low solubility of drugs and nutraceuticals in water decreases their bioavailability, which poses a serious challenge to the biotechnology industry. To improve this, several mixtures have been proposed. Here, the solubility and antioxidant capacity of quercetin in binary mixtures of oleic acid with geraniol and cinnamyl alcohol are determined. As a preliminary step, phase changes and thermophysical properties are discussed and modelled with the PC-SAFT EoS. The densities were between 6% at 283.15 K and 11% at 338.15 K lower than those of water. The surface tensions and viscosities were moderate and also decreased as the temperature increased. The equation of state correctly predicted the density and heat capacity, with average deviations less than 0.32% and 1.9%, respectively. The solubility of quercetin was favored in both mixtures. A synergistic effect on the antioxidant capacity was observed in the mixture with geraniol, which was the least compact.

1. Introduction

The efficiency of any process involving the transfer of matter or energy is highly influenced by the physicochemical properties of the fluid chosen as the solvent. A density sufficiently differentiated from that of water is necessary in liquid-liquid equilibrium processes. Lower surface tension favors fluid penetration into porous materials and, therefore, increases extraction efficiency. Low-viscosity fluids are also preferred as they allow movement between layers and, consequently, contact of the solvent with the matrices. Another basic aspect that determines the choice of the solvent must be its sustainability, both in its production and subsequent use. The water is the best sustainable solvent for hydrophilic substances due to its abundance and zero toxicity. However, many compounds are insoluble in aqueous solutions, and others react with it. There are conventional organic solvents (VOCs) with adequate values for the properties mentioned above. However, all of them have environmental drawbacks. Their production and use emit a large amount of toxic waste, which ends up in various ecosystems. The problems associated with them led to a strong research movement in the late 20th century in the search for new eco-friendly solvents. Some proposed neoteric solvents are biomass-derived liquids, supercritical fluids, ionic liquids (Ils), and eutectic solvents (ESs). The first three types have proven efficient in different processes [1]. This work is focused on studying the fourth. The first definition of eutectic mixtures dates back to 1884 [2]. They were defined as mixtures that, in a given proportion, exhibit a minimum liquefaction temperature. However, it was the paper published by Abbott in 2003 [3] that first introduced the concept of deep ESs (DESs). The term "deep" was due to the pronounced drop in melting temperature (T_m) observed in the choline chloride:urea system compared to that of pure compounds. Since then, the study of these systems has grown exponentially, and the initial confusion regarding their identity has been clarified. In the paper of Abranches and Coutinho [4], issues related to the nature of the eutectic point are analyzed, and the following definition is proposed: "*A eutectic solvent is a eutectic-type system that is a liquid at a given desired temperature where at least one of its components would, otherwise, be a solid unfit to be applied as a solvent. A deep eutectic solvent is a eutectic solvent whose components present enthalpic-driven negative deviations from thermodynamic ideality*" These systems have often been considered systems similar to Ils but this analogy should be strongly avoided. The DESs are systems prepared through a mixing process, and ILs are compounds resulting from a chemical reaction [5,6]. Five types of DESs have been established based on the nature of their components [7]. Of these, the most interesting, especially for the agri-food applications, are those prepared with natural compounds. These are DESs of type III, which are hydrophilic in nature, and type V, which

* Corresponding author at: Departamento de Química Física, Facultad de Ciencias, Universidad de Zaragoza, Zaragoza, Spain.
E-mail address: martal@unizar.es (M. Artal).

https://doi.org/10.1016/j.molliq.2026.129573
Received 20 February 2026; Received in revised form 8 April 2026; Accepted 9 April 2026
Available online 11 April 2026
0167-7322/© 2026 The Authors. Published by Elsevier B.V. This is an open access article under the CC BY-NC-ND license (http://creativecommons.org/licenses/by-nc-nd/4.0/).

Nomenclature

Acronyms

ESs	Eutectic solvents
C	Cinnamyl alcohol
COa	Cinnamyl alcohol:oleic acid (1:1, in mole ratio)
DESs	Deep eutectic solvents
DPPH	2,2-diphenil-1-picrylhydrazyl
DSC	Differential scanning calorimeter
EoS	Equation of state
Fsp^3	sp^3 carbon fraction
G	Geraniol
GOa	Geraniol:oleic acid (1:1, in mole ratio)
HBA	Hydrogen bond acceptor
HBD	Hydrogen bond donor
MRD	Mean relative deviation
Oa	Oleic acid
Oa ESs	Oleic acid-based eutectic solvents
Oa Ss	Oleic acid-based solvents
PC-SAFT	Perturbed-Chain Statistical Associating Fluid Theory
Q	Quercetin
TPSA	Topological polar surface area, ($Å^2$)

Symbols

M	Molar mass, (g/mol)
p	Pressure, (MPa)
p_c	Critical pressure, (MPa)
T	Temperature, (K)
T_m	Melting temperature, (K)
T_m^{id}	Melting temperature assuming ideal behavior, (K)
T_{cr}	Cristallization temperature, (K)
T_c	Critical temperature, (K)
T_g	Glass transition temperature, (K)
$T_{\alpha\rightarrow\gamma}$	Temperature of the polymorphic transformation of oleic acid α → γ, (K)
$T_{\gamma\rightarrow\alpha}$	Temperature of the polymorphic transformation of oleic acid γ → α, (K)
$T_{cr,\alpha}$	Temperature of the crystallization of metastable α, (K)
ΔH	Enthalpy, (kJ/mol)
ΔH_m	Melting enthalpy, (kJ/mol)
$\Delta H_{cr,\alpha}$	Enthalpy of the crystallization of metastable α, (kJ/mol)
$\Delta H_{\alpha\rightarrow\gamma}$	Enthalpy of the polymorphic transformation of oleic acid α → γ, (kJ/mol)
$\Delta H_{\gamma\rightarrow\alpha}$	Enthalpy of the polymorphic transformation of oleic acid γ → α, (kJ/mol)
ρ	Density, (kg/m^3)
u	Speed of sound, (m/s)
n_D	Refractive index
$C_{p,m}$	Isobaric molar heat capacity, (J/mol·K)
γ	Surface tension, (mN/m)
ν	Kinematic viscosity, (mm^2/s)
η	Dynamic viscosity, (mPa·s)
$u(i)$	Standard uncertainty of the property i
$U_c(i)$	Combined expanded uncertainties (0.95 level of confidence, k=2) of property i
A	Absorbance
A_s	Sample absorbance
A_b	Blank absorbance
A_c	Control absorbance
λ	Wavelength
W	Solubility, ($g_{solute}/g_{solvent}$)
Q_s	Sample composition, (mM)
$\%In$	Percentage of inhibition
IC_{50}	Half maximal inhibitory concentration, (μg/mL)
α_p	Isobaric expansibility, (kK^{-1})
κ_s	Isentropic compressibility, (TPa^{-1})
L_f	Free intermolecular length, (Å)
R_m	Molar refraction, (cm^3/mol)
f_m	Free volume, (cm^3/mol)
V_m	Molar volume, (cm^3/mol)
μ_{JT}	Joule-Thomson coefficient, (K/MPa)
ΔS_S	Entropy of surface, (mN/m·K)
ΔH_S	Enthalpy of surface, (mN/m)
$E_{a,\eta}$	Activation energy of viscous flow, (kJ/mol)

have hydrophobic characteristics. The first ones are composed of a quaternary ammonium salt, usually choline chloride, and one or more metabolites. They are commonly called natural deep eutectic solvents (NADESs), and their applications in various fields have been widely studied [8–10]. The latter are generally composed of non-ionic compounds as terpenes, and carboxylic acids or alcohols. With few exceptions, they present a slight decrease in T_m, behavior close to ideality, which is why they are simply called ESs. Both hydrophilic and hydrophobic ESs have shown their applicability in the food industry [11]. Applications of DESs in the extraction of phenols, polyphenols, phenolic acids, anthocyanins, flavonoids, keratin, cellulose, lignins, and proteins from several natural sources have been reported [12]. Recently, their use in food preservation technologies is being studied [13–15]. Their efficacy as environmentally friendly solvents in the detection and extraction of contaminants present in food [16–18], in the extraction of bioactive compounds from natural matrices [19–22], and in improving the solubility of poorly water-soluble drugs and nutraceuticals such as quercetin (Q) [23] is highlighted. Regarding the last application, it must be taken into account that mixtures containing bioactive compounds may show synergies in their properties. For example, both geraniol and oleic acid are good permeant agents, so their combined action enhances the action of APIs that need to cross the dermis [24]. In addition, obtaining a liquid formulation with a higher concentration of the active ingredient, which also includes beneficial properties characteristic of the solvent components, improves the final product. This type of study is beyond the scope of this paper but adds interest to the industrial implementation of these systems. One of the advantages of the eutectic mixtures is their high degree of tunability through appropriate selection of their composition, achieving optimal chemical and physical properties for each application. To this end, the experimental determination of these properties, and the development of thermodynamic tools to predict their values, is essential for their implementation in industry. Several software programs such as SUSSOL or PARIS III [25,26] are being developed to propose eco-friendly solvents for industrial applications. This requires a comprehensive database of thermophysical properties of fluids. This work aims to contribute to expanding this knowledge. Specifically, mixtures of oleic acid (Oa) and geraniol (G) or cinnamyl alcohol (C) are characterized, including their solvent capacity for quercetin. Geraniol ((E) 3,7-dimethyl-2,6-octadien-1-ol) is an acyclic monoterpene alcohol with a hydrophobic character and floral fragrance. It has traditionally been obtained by extracting from different plants such as *Cymbopogon martinii* and *Thymus daenensis*. Currently, its production involves the use of microorganisms such as genetically modified *Escherichia coli*. This compound has beneficial health properties due to its anti-inflammatory and antioxidant properties. It prevents metabolic and heart diseases and is a good neuroprotective and anticancer agent. More extensive information about the properties of geraniol can be found in the work of Singh et al. [27]. Cinnamyl alcohol ((2E)-3-

phenylprop-2-en-1-ol) is an α,β-unsaturated alcohol of interest in fine chemicals as an intermediate compound in the cosmetic and pharmaceutical industries. For instance, it is used as a deodorant due to its sweet, spicy, and hyacinth smell, and a raw material in the synthesis of the antidepressant reboxetine [28,29]. It has also shown anti-inflammatory and anti-oxidative activities in the treatment of sepsis [30]. Small quantities can be extracted from various resins and cinnamon. Larger quantities are usually obtained by chemical synthesis through the selective hydrogenation of cinnamaldehyde [31]. Oleic acid ((9Z)-octadec-9-enoic acid) belongs to the group of unsaturated fatty acids with a single double bond in the ninth position at the end of the terminal methyl group. It is obtained primarily from plants, with olive, camellia seeds, and avocado being the main sources. The Oa content in the first two sources goes up to 83% and up to 68% in the third. These values decrease in sources of animal origin. The fat of farm animals has a percentage of up to 44% and salmon, 30%. Its health benefits have been known since ancient times. It reduces cardiovascular risks, preserves neurological function, and is a potent anti-inflammatory and antioxidant [32]. Additional characteristics, such as its plasticizing and antimicrobial properties, make it a good candidate for applications related to film preparation in the agri-food industry [33]. In the cosmetics and pharmaceutical industries, oleic acid is used as a solvent, drug carrier, liposomal formulation, and emulsifier. It improves drug bioavailability and therapeutic efficacy. All of this has led to a strong recommendation for its inclusion in the diet and an exponential increase in consumption [34]. With a compound annual growth rate (CAGR) of 5.8% between 2024 and 2034, demand for the compound is estimated to reach $1126.3 million by 2034 [35]. Quercetin (*2-(3,4-dihydroxyphenyl)-3,5,7-trihydroxychromen-4-one)* is another compound whose consumption is highly recommended. It belongs to the flavonoid group and is present in high concentrations in fruits and vegetables. Among other properties, it has been observed to improve endothelial function, promote lipid metabolism, have antibacterial, neuroprotective, and antineoplastic properties, and mitigate oxidative stress [36]. These benefits enhance its marketing as a nutraceutical that allows for daily intake of flavonoids. Nevertheless, flavonoids are compounds with very low solubility in aqueous solutions, presenting low bioavailability and stability [37]. Therefore, alternative commercial products that improve these aspects are required [38]. The oleic acid-based ESs (Oa ESs) proposed in this article have been little studied in the literature. The only work found was that published by Pitacco et al. [39]. The authors measured the solid-liquid balance of the geraniol:oleic acid system and the ability of a mixture of given composition to extract astaxanthin from yeast. However, their results are not comparable to ours since their mixtures had a significant water content (2.6 wt%). Other geraniol-based eutectic mixtures containing carboxylic acids as decanoic and octanoic acids have been studied as surfactants and extractants [40,41]. No studies were found that validate thermodynamic models that would allow predicting the behavior of GOa and COa in different scenarios. The latter is of vital importance in the design and optimization of industrial processes.

In this paper, two equimolar mixtures of oleic acid and geraniol or cinnamyl alcohol are analyzed in a temperature range, and at the pressure of 0.1 MPa. The article begins with a description of the compounds and the procedures used to prepare the mixtures and measure the various experimental properties. The models and correlations applied throughout the discussion of results are included in the subsequent section. The last section is divided into the analysis of the results corresponding to the phase changes and thermophysical properties of both oleic acid-based solvents, their ability to dissolve quercetin, and their influence on the antioxidant capacity of quercetin.

2. Materials and methods

2.1. Chemicals

The chemicals used to prepare the hydrophobic solvents (Oa Ss) and their acronyms were oleic acid (Oa), geraniol (G), and cinnamyl alcohol (C). In addition, quercetin (Q) was used in the study of the solubility and 2,2-diphenil-1-picrylhydrazyl (DPPH), and in the measurement of the antioxidant capacity. No purification process was applied to them after the commercial supply. The structures and characteristics of these compounds are reported in Table S1 (supplementary material).

2.2. Preparation of the hydrophobic mixtures

The fluids studied were the binary mixtures of Oa and G or C of composition, (1:1), in molar ratio. These compositions were chosen because most studies of eutectic systems include them, thus allowing for a comparison between them. Furthermore, accurate modeling of this mixture enables a reliable prediction of the behavior of the system at other compositions. To refer to them in the manuscript, we used the acronyms GOa and COa, respectively. The procedure for preparing the mixtures was as follows. First, appropriate amounts of each component of the binary mixture were weighed with a Sartorius PB210S balance ($u(m)=1{\cdot}10^{-4}$ g). Simultaneously stirring and soft heating (323K) were then applied to the flask until the liquid mixture was homogeneous. The mixtures were cooled slowly and no crystallization was observed in any sample. The Karl-Fischer method (automatic titrator Crison KF 1S-2B) was used to measure the water content, which was less than 300 ppm. Table 1 lists a description of both hydrophobic mixtures studied in this work. The calculated molar mass of each mixture ($M_{Oa\ Ss}$) was calculated as the half-sum of the molar masses of the pure components owing to the equimolar composition. Namely, $M_{GOa}=218.36$ g/mol, and $M_{COa}=208.31$ g/mol.

2.3. Phase change

Properties of phase change as glass transition temperature (T_g), melting temperature (T_m), crystallization temperature (T_{cr}), melting enthalpy (ΔH_m), and crystallization enthalpy (ΔH_{cr}) were determined with a differential scanning calorimeter (TA Instruments DSC Q2000) equipped with an RCS cooling system. The calibrations of the temperature and heat flow were performed with a standard of Indium. The uncertainties were estimated from the differences between the expected values of the standard and those from the calibration and the values were $u(T)=0.5$ K and $u(\Delta H)=1$ kJ/mol. Samples with a mass between 5 and 10 mg were placed in an aluminum dish. They were cooled to 213 K and then heated to 313 K at a rate of 3 K/min. The reported temperatures

Table 1
Properties of phase change of the mixtures characterized. Temperature of glass transition (T_g), temperature ($T_{\alpha\to\gamma}$) and enthalpy ($\Delta H_{\alpha\to\gamma}$) of the polymorphic transformation of oleic acid α → γ, temperature ($T_{\gamma\to\alpha}$) and enthalpy ($\Delta H_{\gamma\to\alpha}$) of the polymorphic transformation of oleic acid γ → α, melting temperature (T_m) and enthalpy (ΔH_m), temperature ($T_{cr,\alpha}$) and enthalpy ($\Delta H_{cr,\alpha}$) of the crystallization of metastable α.

Phase change property	Geraniol:oleic acid (1:1)	Cinnamyl alcohol:oleic acid (1:1)
T_g/K	267.92	–
$T_{\alpha\to\gamma}$/K	257.19	258.28
$T_{\gamma\to\alpha}$/K	261.64	260.84
T_m/K	274.05	280.5
$T_{cr,\alpha}$/K	266.14	271.92
$\Delta H_{\alpha\to\gamma}$/(kJ/mol)	0.88	5.3
$\Delta H_{\gamma\to\alpha}$/(kJ/mol)	1.0	2.1
ΔH_m/(kJ/mol)	2.1	13.9
$\Delta H_{cr,\alpha}$/(kJ/mol)	5.1	10.2

correspond to the maximum peak because of the asymmetric peak shapes.

2.4. Thermophysical characterization

The measurement of density (ρ), speed of sound (u), refractive index (n_D), isobaric molar heat capacity ($C_{p,m}$), surface tension (γ), and kinematic viscosity (ν) was performed using well-known devices. Table S2 lists the type, standard and combined uncertainties, and several details of procedure of each apparatus. Uncertainties are also included in the tables containing the data. The measurements were taken in triplicate and the value given in the table is the average of them. All experimental set-up were validated with standard fluids (Antón et al., 2017) and the mean relative deviations ($MRD(Y)$) calculated in the comparison with literature data were $MRD(\rho)$=0.004%, $MRD(u)$=0.026%, $MRD(n_D)$=0.007%, $MRD(C_{p,m})$=0.028%, $MRD(\gamma)$=0.21%, and $MRD(\nu)$=0.28%.

2.5. Solubility measurements

The shake-flask method [42] was used to determine the thermodynamic solubility of Q in the mixtures previously prepared. An excess of Q was added to 5 mL of solvent so the mixture remained supersaturated. The flask thermostatted at 298 K was under constant agitation for 12 h. After, the samples were centrifuged (2390 xg, 30 min) and filtered (PES syringe filters, 0.22 mm) before analysis. The quantification of solubilized quercetin (W_Q) was carried out by UV-VIS spectroscopy using a VWR 6300 PC double-beam equipment (u(λ) = 0.2 nm). The samples were diluted in ethanol (≥99.5%) and the maximum absorbance (A_{374}) was taken and compared with a calibration curve previously obtained (Table S3, Fig. S1). Each experiment was repeated three times and each sample was diluted in ethanol twice. Therefore, each result was the average value of six data. The uncertainty calculated was $u(W_Q)$=3.6·10^{-6} (g_Q/g_s).

2.6. DPPH assay

The antioxidant capacity of different systems was measured using the method of Blois [43]. The DPPH is a very stable radical due to the delocalization of the free electron in the nitrogen atom. This fact is also the reason why its solution in ethanol has an intense purple color and a maximum absorbance at 517 nm. When this solution is mixed with a substance capable of donating a hydrogen atom or electron, the DPPH is reduced to hydrazine (DPPH-H), and the color changes from purple to pale yellow with the visible band disappearing. So, the reaction can be monitored by UV–vis spectroscopy at 517 nm. We used the spectrophotometer described in the Section 2.5. In the assays, the compositions of the solutions were adequate to follow the Beer-Lambert law. Six dilutions of the sample to study in ethanol (≥99.5%) at different compositions (Q_s) were prepared. A volume of 0.2 mL of each above solution was mixed with 1.8 mL of ethanol and their absorbances were measured as blank (A_b). Also, 0.2 mL of each solution Q_s was added to 1.8 mL of ethanolic DPPH solution (0.08 mM) previously prepared. The mixtures were stored in darkness for 30 min and the absorbance (A_s) was measured. Finally, the absorbance of a mixture composed of 0.2 mL of ethanol and 1.8 mL of the ethanolic DPPH solution was determined (A_c). This value was used as a parameter to monitor the stability of the DPPH concentration. The percentage of inhibition of DPPH (%In_{DPPH}) was calculated as follows:

$$\%In_{DPPH} = \frac{A_c - (A_s - A_b)}{A_c} \tag{1}$$

The half maximal inhibitory concentration ($IC_{50}/(\mu g/mL)$), defined as the concentration required for the 50% inhibition of initial DPPH, is a parameter very used in the literature. To calculate it, %In_{DPPH} versus Q_s was linearly fitted:

$$\%In_{DPPH} = A + BQ_s \tag{2}$$

3. Theory

3.1. PC-SAFT EoS

A more comprehensive description of PC-SAFT can be found in the papers published by Gross and Sadowski [44,45]. A brief summary is presented here. This model describes the Helmholtz energy ($\tilde{a}$) as the sum of several terms: the contribution of ideal gas ($\tilde{a}^{id}$), the repulsive term represented by the hard-chain reference system ($\tilde{a}^{hc}$), and the attractive terms of dispersive ($\tilde{a}^{dis}$) and association ($\tilde{a}^{assoc}$) interactions. The equations are:

$$\tilde{a} = \tilde{a}^{id} + \tilde{a}^{hc} + \tilde{a}^{dis} + \tilde{a}^{assoc} \tag{3}$$

$$\tilde{a}^{hc} = m\tilde{a}^{hs} - (m-1)\ln g^{hs} \tag{4}$$

$$\tilde{a}^{dis} = -2\pi\rho m^2\left(\frac{\varepsilon}{kT}\right)\sigma^3\sum_{i=0}^{6}\left[a_{0i} + \frac{m-1}{m}a_{1i} + \frac{m-1}{m}\frac{m-2}{m}a_{2i}\right]\eta^i - \pi\rho mkT\left(\frac{\partial\rho}{\partial p}\right)_{hc} m^2\left(\frac{\varepsilon}{kT}\right)^2\sigma^3\sum_{i=0}^{6}\left[b_{0i} + \frac{m-1}{m}b_{1i} + \frac{m-1}{m}\frac{m-2}{m}b_{2i}\right]\eta^i \tag{5}$$

$$\tilde{a}^{assoc} = \sum_A\left[\ln\left(1+\rho X^A\Delta\right)^{-1} - \frac{\left(1+\rho X^A\Delta\right)^{-1}}{2}\right] + \frac{1}{2}S \tag{6}$$

$$\Delta = \kappa^{A_iB_i}\sigma^3 g^{hs}\left[\exp\left(\frac{\varepsilon^{A_iB_i}}{kT}\right) - 1\right] \tag{7}$$

where $a_{0i}, a_{1i}, a_{2i}, b_{0i}, b_{1i}$, and b_{2i}, are called *universal constants* and their values were obtained from the thermodynamic properties of *n*-alkanes. Also, m is the chain segment number, g^{hs} is the radial pair distribution function of the segments, $\tilde{a}^{hs}$ is the Helmholtz energy of the hard sphere, ρ is the density, p is the pressure, T is the temperature, σ is the segment diameter, ε is the segment energy, η is the packing fraction, X^A is the fraction of unbonded monomers, Δ is the tendency to form *n*-mers, $\kappa^{A_iB_i}$ is the association volume, $\varepsilon^{A_iB_i}$ is the association energy, and S is the number of associated sites of the compound. Therefore, 3 geometric parameters (m, σ and ε), two association parameters ($\kappa^{A_iB_i}$ and $\varepsilon^{A_iB_i}$), and an association scheme are needed to characterize each pure compound capable of associating. They are usually calculated from data of thermodynamic properties of the pure compounds. For Oa and G, the parameters were taken from literature [46,47]. For C, they were estimated in this work. To do this, the objective function included data of ρ and $C_{p,m}$ of pure C at a pressure of 0.1 MPa and in the temperature range of 303 to 338 K.

To model mixtures, the mixing rules are needed. We used the following:

$$\sigma_{ij} = \left(\sigma_i + \sigma_j\right)/2 \tag{8}$$

$$\varepsilon_{ij} = \sqrt{\varepsilon_i\varepsilon_j}\left(1 - k_{ij}\right) \tag{9}$$

$$\kappa^{A_iB_j} = \sqrt{\kappa^{A_iB_i}\,\kappa^{A_jB_j}} \tag{10}$$

$$\varepsilon^{A_iB_j} = \left(\varepsilon^{A_iB_i} + \varepsilon^{A_jB_j}\right)/2 \tag{11}$$

where the subscripts i and j refer to each of the compounds present in the mixture, and k_{ij} is the binary interaction parameter. In the predictive version of the model, the one used in this work, the parameter is null, k_{ij}=0.

3.2. Estimation of the isobaric molar heat capacity

The $C_{p,m}$ of mixtures can be estimate from critical properties with the correlation of Taherzadeh et al. [48]:

$$C_{p,m} = A + 132.27\ T^{1/4}, \tag{12}$$

$$A = 3.8 \bullet 10^{-4}\frac{M_{Oa\ Ss}^3}{p_c^6} + 6.3 \bullet 10^{-5}M_{Oa\ ES}^{2\omega} - \frac{24577.4}{M_{Oa\ Ss}} - 94.9, \tag{13}$$

where T is the temperature, $M_{Oa\ Ss}$ is the molar mass (Section 2.2), p_c is the critical pressure, and ω is the acentric factor of each characterized Oa ESs. The last two parameters were estimated from the Lee-Kesler (LK) mixing rules:

$$p_c(\text{bar}) = (0.2905 - 0.0850\omega)\frac{83.1447T_c}{V_c}, \tag{14}$$

$$\omega = \sum_{n=1}^{3} x_n\omega_n, \tag{15}$$

$$V_c(\text{mL/mol}) = \sum_{n=1}^{3}\sum_{m=1}^{3} x_n x_m V_{c,mn}, \tag{16}$$

$$T_c(\text{K}) = \frac{1}{V_c^{0.25}}\sum_{n=1}^{3}\sum_{m=1}^{3} x_n x_m V_{c,mn}^{0.25} T_{c,mn}, \tag{17}$$

$$V_{c,mn}(\text{mL/mol}) = \frac{1}{8}\left(V_{c,n}^{1/3} + V_{c,m}^{1/3}\right)^3, \tag{18}$$

$$T_{c,mn}(\text{K}) = \left(T_{c,n}T_{c,m}\right)^{0.5}, \tag{19}$$

where the subscripts n and m represent each component, and mn is the subscript indicating binary interaction term. T_c and V_c are the critical temperature and critical volume of the Oa Ss.

3.3. Estimation of the critical temperature

The T_c of GOa and COa were calculated with PC-SAFT EoS (Eqs. (3)–(11)) and the LK mixing rules (Eqs. (14)–(19)). In addition, the equations of Gugghenheim [49] and Eötvos [50] were used:

$$\gamma = \gamma_0(1 - T/T_c)^{11/9}, \tag{20}$$

$$\gamma(M_{Oa\ Ss}/\rho)^{2/3} = K(T_c - T), \tag{21}$$

where γ_0 is the surface tension at 0 K, $M_{Oa\ Ss}$ is the molar mass of the Oa ES, and γ and ρ are the surface tension and density at the temperature T.

3.4. Estimation of the surface tension

The following correlations were chosen for their simplicity and because they only require values of the mixture properties. The equation of Papazian [51] correlates n_D and γ, as follows:

$$\gamma = A_1\left(\frac{n_D^2 - 1}{2n_D^2 + 1}\right) + B_1, \tag{22}$$

where A_1, and B_1 are the fit coefficients. Furthermore, the equations of Pelofsky and Murkerjee [52] correlate γ and η:

$$\ln\gamma = \ln A_2 + \frac{B_2}{\eta}, \tag{23}$$

$$\ln\gamma = \ln A_3 + \frac{B_3}{3}\ln\eta, \tag{24}$$

where A_2, A_3, B_2, and B_3 are the fit coefficients.

4. Results and discussion

4.1. Phase change

In this first subsection, we provide comprehensive insight into the thermal behavior of the eutectic mixtures characterized. Knowing phase change parameters is important in industry because they indicate the temperature window in which the solvent is in the liquid phase, as well as the heat exchanged in the process. In the GOa system, two exothermic and three endothermic peaks were observed (Fig. S2a). The first exothermic peak can be attributed to the crystallization of a metastable α-phase. In pure Oa, this fact typically occurring at $T_{cr,\alpha}$=272.15 K [53]. However, the incorporation of G likely disrupts the crystalline packing of Oa, promoting the formation of a eutectic mixture and consequently lowering the crystallization temperature [47]. The second exothermic event corresponded to a reversible polymorphic transformation from the α- to γ-phase. The exothermic and endothermic values in oleic acid-based systems are commonly reported at $T_{\alpha\rightarrow\gamma}$=262.15 K, and $T_{\gamma\rightarrow\alpha}$=268.15 K [53,54]. Furthermore, the presence of G in the mixture appears to enhance the amorphous character of the system, leading to a glass transition that manifests as a subtle shoulder at the second endothermic peak. The final endothermic peak would then be associated with the melting of the GOa eutectic mixture. The corresponding transition temperatures and associated enthalpies including those related to the glass transition, α↔γ polymorphic transformations, melting, and crystallization of the metastable α phase are summarized in Table 1. In contrast, the DSC thermogram of the COa system (Fig. S2b) displayed two exothermic peaks corresponding to the crystallization of the metastable α-phase and the α → γ polymorphic transformation of Oa. Two sharp endothermic peaks were also observed, attributed to the reverse γ → α phase transition and the melting of the COa eutectic mixture, respectively. Due to the higher crystallization propensity between C and Oa, no glass transition was detected in the COa system. A detailed summary of the thermal transition temperatures and associated enthalpic changes is presented in Table 1. The solid-liquid phase diagram of GOa was studied by Pitacco et al. [39]. The T_m value published was higher than ours. It is worth noting that T_m of pure G given by these authors, 258 K, was also much higher than that published by Štejfa et al. [55], 183 K. These differences could be due to the different water content; Pitacco et al. reported a 2.6 wt%.

As mentioned in the introduction, classifying a eutectic mixture as DES implies a significant decrease in T_m compared to the value it would have for its assumed ideal behavior (T_m^{id}). For GOa, the lack of reliable values for the melting properties of pure G makes it impossible to reliably calculate the T_m^{id} of the mixture, and consequently, its classification. Therefore, the GOa mixture will not be referred to as a eutectic mixture throughout this manuscript. On the other hand, T_m^{id}(COa) = 291.5 K. Considering the experimental value (Table 1), a decrease of 11 K has occurred and, therefore, COa can be classified as ES.

4.2. Thermophysical properties

The thermodynamic and transport properties of a solvent determine the operational design of industrial processes and their effectiveness. Here, results of six properties measured at temperatures from 283.15 K to 338.15 K in intervals of 2.5 K are discussed. All the values are reported in the supplementary file (Tables S4-S5). In addition, Table 2 lists the experimental and calculated property data at 293.15 K to make it easier to follow the discussion. As is usual in liquid systems, a linear equation was used to correlate the thermodynamic properties with temperature and an exponential equation was used for the transport one. The equations and the coefficients of the relationships are summarized in Table 3.

Standard uncertainties are: $u(T)$=0.005 K for density and speed of sound and 0.01 K for the rest of properties; $u(p)$=0.5 kPa. The combined expanded uncertainties (0.95 level of confidence, k=2) are $U_c(\rho)$=0.05

Table 2
Thermophysical properties of the mixtures characterized at $T = 293.15$ K and $p = 0.1$ MPa.

Property	Geraniol:oleic acid (1:1)	Cinnamyl alcohol:oleic acid (1:1)
Density, ρ/(kg/m^3)	887.45	937.20
Speed of sound, u/(m/s)	1436.42	1480.90
Refractive index, n_D	1.46695	1.49621
Isobaric molar heat capacity, $C_{p,m}$/(J/mol·K)	462	436
Surface tension, γ/(mN/m)	31.13	33.54
Dynamic viscosity, η/(mPa·s)	19.59	33.64
Isobaric expansibility, α_p/(kK^{-1})	0.798	0.765
Isentropic compressibility, κ_s/(TPa^{-1})	546.13	486.54
Molar refraction, R_m/ (cm^3/mol)	68.38	64.88
Free volume, f_m/ (cm^3/mol)	178.07	157.13
Joule-Thomson coefficient, μ_{JT}/(K/MPa)	−0.408	−0.395
Entropy of surface, ΔS_S/(mN/m·K)	0.0853	0.0824
Enthalpy of surface, ΔH_S/(mN/m)	56.13	57.69
Activation energy of viscous flow, $E_{a,\eta}$/(kJ/mol)	27.80	34.47

Table 3
Fitting parameters (A_Y, B_Y, C_Y) and regression coefficients, R^2, of the experimental thermophysical properties of the mixtures characterized.[a]

Property	Mixtures	A_Y	B_Y	C_Y	R^2
Density[b], ρ /(kg/m^3)	GOa	1095.07	−0.7082		1
	COa	1147.45	−0.7173		1
Speed of sound[b], u/(m/s)	GOa	2439.40	−3.4197		0.9998
	COa	2465.00	−3.3556		0.9997
Refractive index[b], n_D	GOa	1.58327	$-3.97\cdot10^{-4}$		1
	COa	1.61534	$-4.06\cdot10^{-4}$		1
Isobaric molar heat capacity[b], $C_{p,m}$/(J/mol·K)	GOa	164.72	1.0147		1
	COa	193.88	0.8268		1
Surface tension[b], γ/(mN/m)	GOa	56.09	−0.0853		0.9990
	COa	57.67	−0.0824		0.9995
Dynamic viscosity[c], η/(mPa·s)	GOa	0.04045	982.02	134.30	0.9997
	COa	0.07298	779.72	166.02	0.9998

[a] GOa is geraniol:oleic acid (1:1), and COa is cinnamyl alcohol:oleic acid (1:1).
[b] $Y = A_Y + B_Y T$
[c] $Y = A_Y \exp\left[\frac{B_Y}{T - C_Y}\right]$

kg/m^3; $U_c(u)$=0.5 m/s; $U_c(n_D)=2\cdot10^{-5}$; $U_c(C_{p,m})$=1%; $U_c(\gamma)$=1%; $U_c(\eta)$=1%; $U_c(\alpha_p)$=0.04 kK^{-1}; $U_c(\kappa_s)$=0.22 TPa^{-1}; $U_c(R_m)$=0.004 cm^3/mol; $U_c(f_m)$=0.03 cm^3/mol; $U_c(\mu_{JT})$=1%; $U_c(\Delta S_S)$=0.001 mN/m·K; $U_c(\Delta H_S)$=0.06 mN/m.

4.2.1. Density

Both studied mixtures were suitable to use in liquid-liquid extractions owing to the differences between their ρ values and those of the water were higher than 50 kg/m^3. The COa mixture was 5.5% denser than GOa due to the planar structure of the aromatic ring present in C. Our group previously characterized similar mixtures of oleic acid with other components of essential oils as thymol, l-menthol, eugenol, and linalool [56]. With the exception of the mixture with eugenol, the ρ values of COa were higher than that of the others. On the other hand, GOa was the least dense mixture. The higher the temperature, the greater the thermal agitation, which causes a decrease in density (Fig. 1a). The expansion capacity of the fluid as the temperature increases is called isobaric expansibility (α_p) and is calculated as:

$$\alpha_p = -\frac{1}{\rho}\left(\frac{\partial\rho}{\partial T}\right)_p \tag{25}$$

The values of this property were highest in the mixture with G, showing that it was less compact than that with C (Table 2, Fig. 2a).

The increase in thermal energy facilitates the expansion of liquids, so the temperature coefficient of this property is positive. The values were $(\partial\alpha_p/\partial T)$=(65 ± 0.04)·10^{-4} and (60 ± 0.04)·10^{-4} kK^{-2} for GOa and COa, respectively. Being able to predict the value of ρ of a mixture at any composition and temperature is a very useful tool in the design of industrial processes. For this purpose, the equations of state are often used but they must be previously validated. Here, we use PC-SAFT EoS as described in the Section 3.1, and with the parameters listed in Table S6. The values predicted of ρ were in agreement with those measured and the mean relative deviations were MRD_ρ(GOa) = 0.32% and MRD_ρ(COa) = 0.21%. A graphical comparison is presented in Fig. S3a.

4.2.2. Speed of sound

The speed of sound propagation in a material is indicative of its compaction. The more compact, the higher the value of u. The aromatic ring in C favored compaction, and the values of COa were, on average, 45 m/s greater than those of GOa. The mixture with C was also more compact than the other Oa Ss studies formerly published [56]. The increase in the thermal energy increases the free volume in the fluids so u decrease with T increases (Fig. 1b). The isentropic compressibility (κ_s) is defined as the capacity of a fluid to be compressed without changing its entropy and is calculated as:

$$\kappa_S = 1/\rho u^2 \tag{26}$$

In agreement with the previous results, the values of this property were higher in GOa and increased with T (Table 2, Fig. 2b). The temperature coefficients were $(\partial\kappa_S/\partial T)$= (3.43 ± 0.04) TPa^{-1}·K^{-1} for GOa and (2.89 ± 0.03) TPa^{-1}·K^{-1} for COa. From κ_S property, an equation to estimate of the free intermolecular length (L_f) was proposed by Jacobson [57]:

$$L_f = (91.368 + 0.3565T)10^8\sqrt{\kappa_S} \tag{27}$$

The values ranged from 0.427 Å to 0.564 Å for GOa and from 0.403 Å to 0.529 Å for COa. They increased with T as κ_S.

4.2.3. Refractive index

The n_D is defined as the ratio of the speed of light in vacuum to the speed of light in a fluid. Light travels faster in vacuum, so a fluid with a larger free volume (f_m) will have a lower n_D value. In our mixtures, COa had the highest values showing higher compaction. The f_m increases with T so the slope of the $n_D - T$ relationship is negative (Table 3, Fig. 1c). The equation of the Lorentz-Lorentz allows to calculate the molar refraction (R_m) from data of the molar volume ($V_m = M/\rho$) and n_D as follows:

$$R_m = \frac{M}{\rho}\frac{(n_D^2 - 1)}{(n_D^2 + 2)} \tag{28}$$

The higher the R_m values of a fluid, the greater its affinity for highly polarizable substances. In this work, the values were higher for GOa and increased with T (Table 2, Fig. 2c). The temperature coefficients were $(\partial R_m/\partial T)$=(4.51 ± 0.02)·10^{-3} cm^3/mol·K for GOa and (4.43 ± 0.05)·10^{-3} cm^3/mol·K for COa. Considering that R_m is also related to the volume occupied by a mole of hard cores of the molecules, the f_m can be calculated as the subtraction between the V_m and R_m. From this, the percentage of the free volume was estimated and compared with data for other OA ESs [56]. The percentage was of 72.5% for GOa and 70.8% for COa. The first one was similar to those data found for mixtures with non-aromatic compounds. The second was lower than all of them.

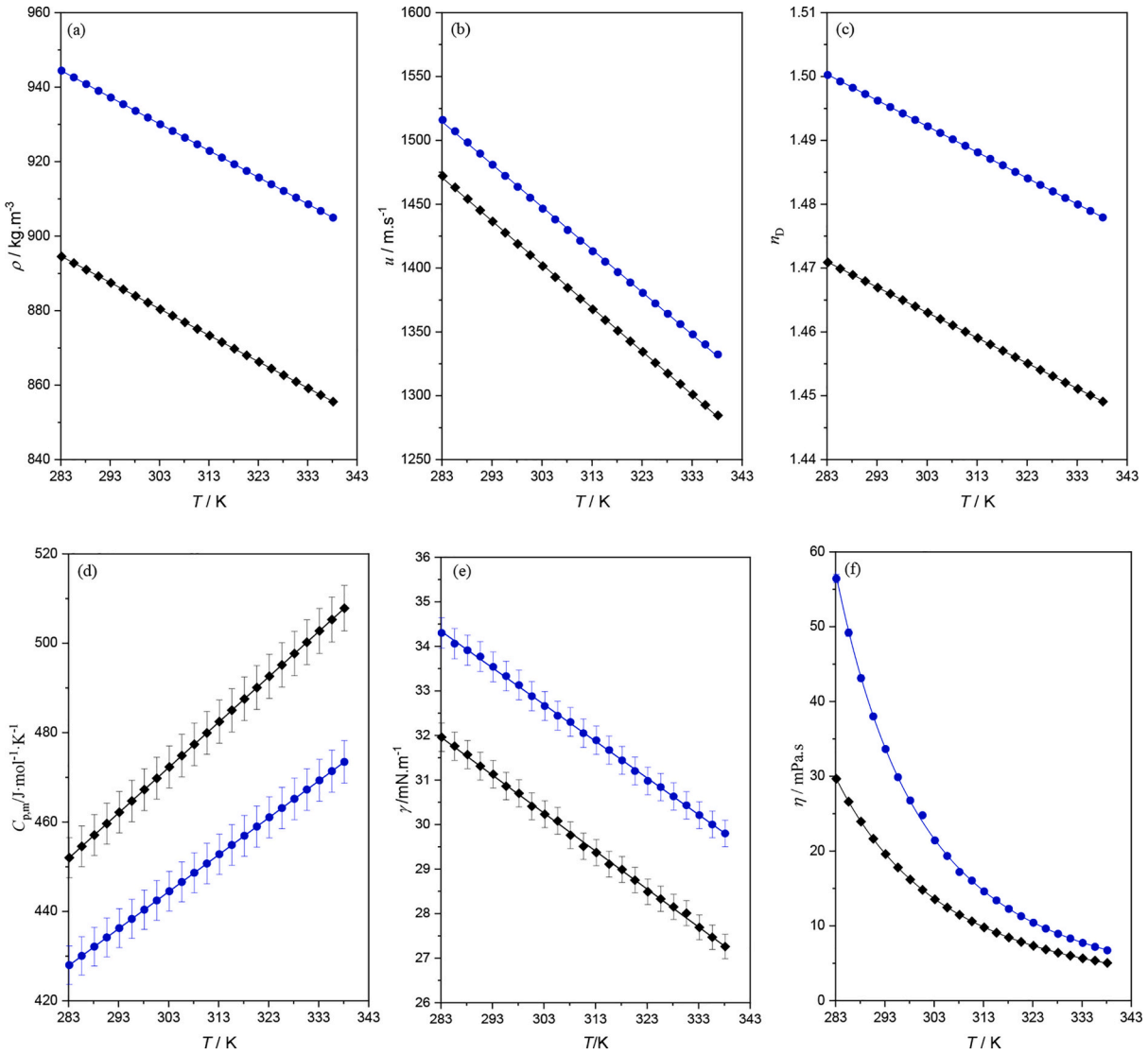

Fig. 1. Experimental properties of the mixtures studied at p=0.1 MPa, and at various temperatures (T). (a), Density (ρ); (b), Speed of sound (u); (c), Refractive index (n_D); (d), Isobaric molar heat capacity ($C_{p,m}$); (e), Surface tension (γ); and (f) Dynamic viscosity (η). (◆), (—), Geraniol:oleic acid (1:1) (GOa); (●), (– –), Cinnamyl alcohol:oleic acid (1:1) (COa). Points, experimental values; lines, correlated data.

4.2.4. *Isobaric molar heat capacity*

The $C_{p,m}$ values of GOa were higher than those of the COa according to the greater molar mass of the first and the difference increased with T (Fig. 1d). The $C_{p,m}$ sequence was in agreement with that previously published for other Oa ESs [56]. This property can be predicted with the PC-SAFT EoS (Section 3.1) whose validity for the two systems has already been demonstrated from the volumetric behavior (Section 4.2.1). In addition, $C_{p,m}$values at different temperatures can be correlated from the molar mass, acentric factor and critical properties data of the pure compounds, and by applying mixing rules (Section 3.2). For GOa, the results obtained agreed with the experimental ones with a mean relative deviation of 1.9% for both methods. For COa, the values obtained from the EoS deviated on average from the experimental ones by 1.4%. In the correlation, the deviation increased up to 13% probably due to inadequate values of the critical properties of pure C. Fig. S3b shows the graphical comparison between experimental and predicted data from EoS as a function of T. Also, the Joule-Thomson coefficient (μ_{JT}) was calculated from $C_{p,m}$ and ρ data at different T as follows:

$$\mu_{JT} = \frac{V_m}{C_{p,m}}\left(T\alpha_p - 1\right) \tag{29}$$

This parameter quantifies the variation in temperature with changes in pressure in an isenthalpic process. The values obtained (Table 2, Fig. 2d) were negative in both mixtures, with a higher absolute value for GOa. The predicted μ_{JT} with PC-SAFT EoS were lower than the experimental ones with a mean relative deviation of 4.31% for GOa, and 6.39% for COa. The graphical comparison can be seen in Fig. S3c.

4.3. *Surface tension*

The γ of a fluid is related to the energy required to increase the surface area of its interface with the air. The more structured a fluid is, the greater this energy. For COa, the values were about 3 mN/m higher than for GOa. This fact was in agreement with the higher compaction observed in the system with the aromatic ring. In relation to the γ published for other Oa Ss [56], COa was the most structured fluid and GOa the least. Structuring is prevented by thermal agitation so the γ decreases with increasing T (Fig. 1e). The liquid-vapor meniscus vanishes at the critical temperature (T_c); i.e. $\gamma \to 0$ at $T \to T_c$. According to this, an estimate of T_c can be made from experimental γ data. We used the Guggenheim and the Eötvos equations (Section 3.3). Tables S7 and S8 report these values and those calculated with the method of Lee-

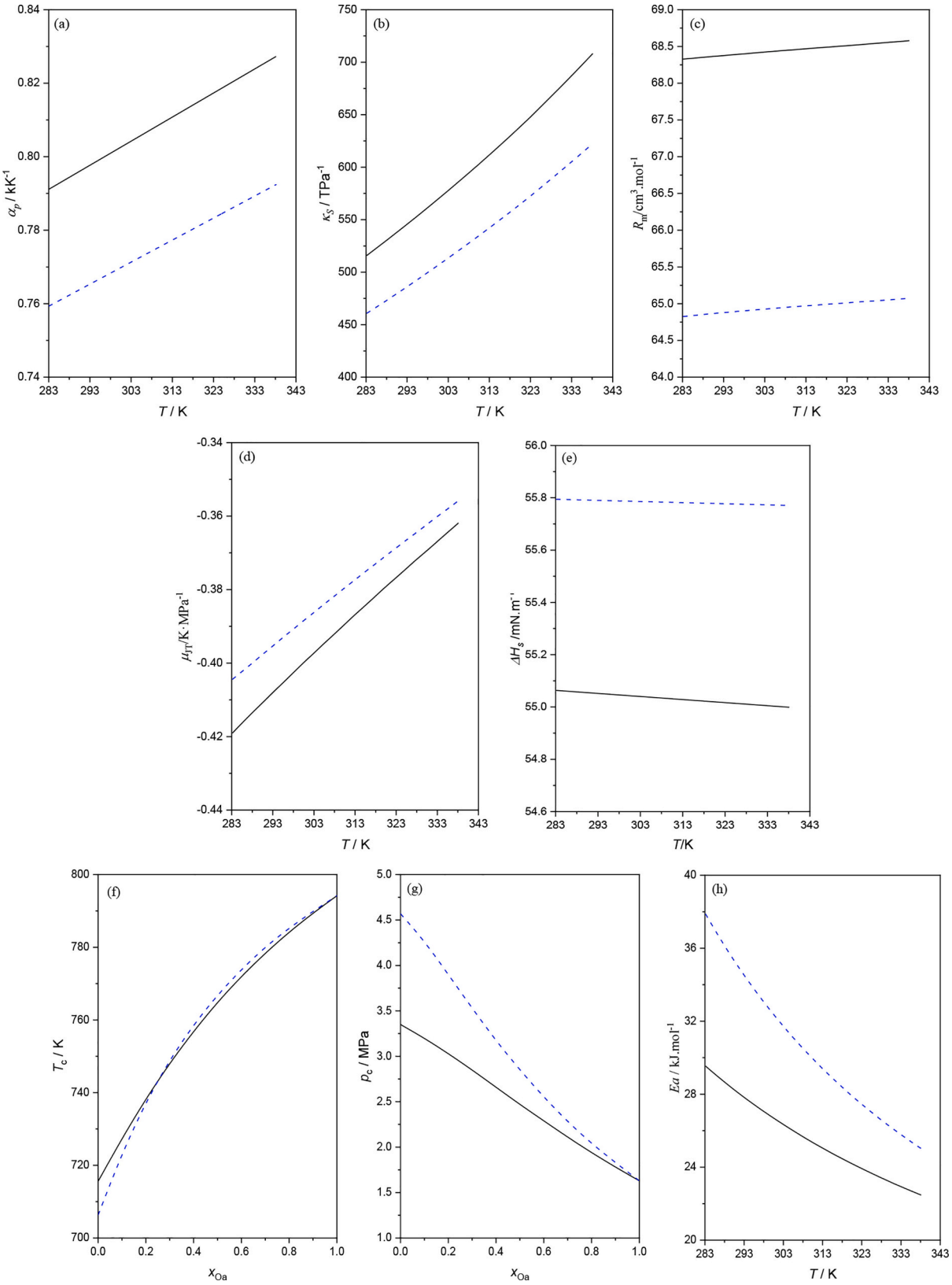

Fig. 2. Calculated properties of the mixtures studied at p=0.1 MPa, and at various temperatures (T). (a), Isobaric expansibility (α_p); (b), Isentropic compressibility, (κ_s); (c), Molar refraction (R_m); (d), Joule-Thomson coefficient (μ_{JT}); (e), Enthalpy of surface per unit of area (ΔH_S); (f) Critical temperature predicted with PC-SAFT EoS (T_c); (g), Critical pressure predicted with PC-SAFT EoS (p_c); and (h), Activation energy of viscous flow ($E_{a,\eta}$). (◆), (—), Geraniol:oleic acid (1:1) (GOa); (●), (– –), Cinnamyl alcohol:oleic acid (1:1) (COa).

Kesler (Section 3.2) and the PC-SAFT EoS (Section 3.1). The critical pressure (p_c) was also calculated with the last two methods. Fig. 2f and g display the critical loci obtained with the EoS. The calculated values of both properties are very useful, since their knowledge is essential in the design of industrial processes but they are difficult (often impossible) to measure experimentally. Thermodynamic properties of surface can be calculated from data of the γ and its behavior with T. They are the entropy (ΔS_s) and the enthalpy (ΔH_S) of surface per unit of area, and the equations are:

$$\Delta S_s = -\left(\frac{\partial \gamma}{\partial T}\right)_p \tag{30}$$

$$\Delta H_S = \gamma - T\left(\frac{\partial \gamma}{\partial T}\right)_p \tag{31}$$

The degrees of freedom of a molecule increase when passing from the bulk of the fluid to the surface, so the process is entropically favored. On the other hand, it is enthalpically unfavored. For GOa, the ΔS_s value was higher and the ΔH_S data were lower than the corresponding to COa (Table 2). The enthalpic contribution slightly decreased with T (Fig. 2e). The intermolecular interactions present in the medium are both the forces that must be overcome to bring a molecule to the surface of the fluid and those responsible for its dielectric constant. The change in symmetry of the forces when a molecule passes from the interior to the surface of a fluid, causes a change in its polarity. Therefore, it is expected that the energy associated with the process is related to the dielectric constant of the medium (or n_D^2 in polar liquids in accord with the Maxwell relation). Accordingly, we applied the linear equation proposed by Papazian (Section 3.4) to the mixtures studied and a good correlation was found (Table 4 and Fig. S4a).

4.3.1. Viscosity

The viscosity of a fluid is indicative of the resistance it presents to move due to friction between the layers of the liquid. High values of this property represent a serious drawback in the design of industrial processes that include material exchanges. In fact, one of the advantages in extraction applications of hydrophobic solvents over hydrophilic ones is their greater fluidity. For the latter, values of the dynamic viscosity (η) up to $5.1{\cdot}10^5$ mPa.s have been measured [58]. The dynamic viscosity is calculated as $\eta{=}\rho\nu$ and is the property that is usually discussed. In literature, the value of 100 mPa.s is reported as the maximum viscosity value to ensure proper operation of the equipment [59]. Our Oa Ss presented viscosities lower than that value in the T range studied. The system with C was the most viscous and the difference in η between both mixtures decreased markedly as T increased (Fig. 1f). Except for the mixture with l-menthol, COa was the most viscous Oa Ss studied to date [56]. On the other hand, GOa was the most fluid. This sequence corresponds to the greater intermolecular interaction exhibited by aromatic compounds, and among non-aromatic compounds, to the greater difficulty of movement between layers of the most branched ones. Usually, the $\eta - T$ relationship is exponential and we used the VFT equation [60]. The expression and the three fitting coefficients (A_Y,B_Y, C_Y) are listed in Table 3. The first coefficient is the viscosity in the absence of thermal energy and therefore corresponds to the contribution to viscosity by solely steric effects. It was much higher in the more compact system. The other two are related to the energy required to overcome intermolecular interactions and allow the calculation of the activation energy of viscous flow as follows:

$$E_{a,\eta} = R\frac{\partial(\ln\eta)}{\partial\left(\frac{1}{T}\right)} = R\left(\frac{B_Y}{\left(\frac{C_Y^2}{T^2} - \frac{2C_Y}{T} + 1\right)}\right) \tag{32}$$

The $E_{a,\eta}$ value of the COa was 31% higher than that of the GOa at 278.15 K and this difference decreased up to 11% at 338.15 K (Fig. 2h). These results are related to the presence of stronger interactions in the first mixture, which are weakened by increasing the thermal energy. Considering that the values of η and γ are indicative of the cohesion between the molecules in a fluid, a relationship between both properties can be expected. We evaluated two equations previously proposed by Pelofsky and Murkerjee (Section 3.4). Table 4 lists the coefficients for both correlations, and a graphical representation is shown in the supplementary material (Fig. S4b, S4c).

Table 4
Fit parameters of the surface tension correlations.

Method	Parameter	Geraniol:oleic acid (1:1)	Cinnamyl alcohol:oleic acid (1:1)
Papazian (Eq. 22)	A_1	679.36	670.51
	B_1	−116.36	−118.13
	R^2	0.9988	0.9995
Pelofsky (Eq. 23)	$\ln A_2$	3.483	3.541
	B_2 / mPa·s	−0.944	−1.061
	R^2	0.982	0.977
Murkerjee (Eq. 24)	$\ln A_3$	3.172	3.278
	$B_3/3$	0.089	0.066
	R^2	0.990	0.984

4.4. Solubility study

The solubility of a solute in a solvent is related to the ability of the solvent to interact with each other. The structural characteristics of the compounds involved and the properties of the mixture are determining factors in the solubilization process. Solutes with flatter structures generate more stable crystals and, consequently, are not very soluble. A high number of hydrogen bond donor (HBD) or acceptor (HBA) sites, a high topological polar surface area (TPSA), and a large hydrophobic region in both the solute and the solvent are factors that favor interactions between them. In addition, using solvents with high free volume and low viscosity, and applying agitation during the process facilitates the diffusion of the solute into the liquid. Table S9 lists the structural properties of the pure compounds used in this work, and the solvent properties have been discussed in Section 4.2. Quercetin has a single rotatable bond and zero sp^3 carbon fraction, so its structure is planar and very stable. Consequently, its solubility in water must be very low. The published value is $W_Q{=}4.3{\cdot}10^{-7}$ (g_Q/g_s) (López et al., 2020). On the other hand, Q has a high number of HBD and HBA sites and TPSA, and medium polarizability. Therefore, it is expected that its solubility will be greater in solvents with greater molar refraction, as those in this work. Considering the structural properties, G has a higher sp^3 carbon fraction (Fsp^3) and number of rotatable bonds than C, which implies a greater capacity to occupy target space. This fact is consistent with the higher f_m percentage obtained in the mixture (Section 4.2.3). Furthermore, its higher R_m and lower η are also factors that could explain the higher solubility value of Q in GOa. Specifically, the values at 298.15 K were $W_Q{=}(5.73 \pm 0.13){\cdot}10^{-4}$ (g_Q/g_s) for GOa, and $W_Q{=}(5.23 \pm 0.05){\cdot}10^{-4}$ (g_Q/g_s) for COa. In a previous work [21], we determined the extraction capacity of astaxanthin from yeast, using GOa and COa, among other ESs, as solvents. In that case, GOa also showed greater affinity than COa. The solubility of Q in eutectic solvents of both hydrophobic and hydrophilic nature have been reported in the literature [23,61–67]. A graphical comparison can be seen in Fig. 3. The values were lower than those found for mixtures with l-menthol, a compound with maximum Fsp^3 ($Fsp^3 = 1$), higher than those published for the rest of the Oa ESs and for most of the hydrophilic compounds. It should be noted that in the latter, the water content in the mixture significantly

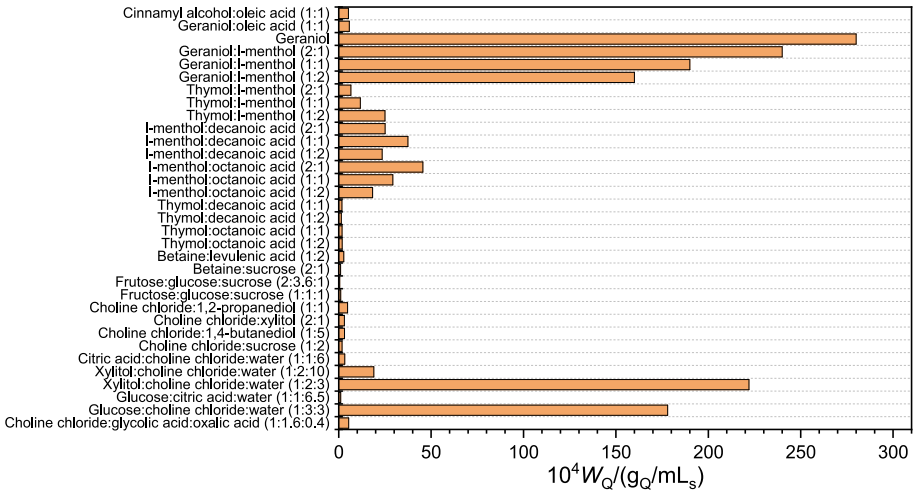

Fig. 3. Comparison between solubility data of Q at 298.15 K in different eutectic mixtures.

influences the solubility.

4.5. DPPH antioxidant capacity

The antioxidant properties of Q and the bioactive properties of G, C, and Oa are well known in the literature [27,32,36,68]. Regarding the DPPH radical, the inhibition percentage (%In_{DPPH}) and the half-maximal inhibitory concentration (IC_{50}), calculated with Eq. 1 and Eq. 2, are the parameters that quantify it. In this section, we evaluate the potential synergy between components in the Q mixtures in GOa and COa by determining both parameters. Because the results of this assay depend heavily on the conditions under which the experiment is performed, it is advisable to check the procedure with a reference sample as ascorbic acid in ethanol [69–71]. This study was also performed for a sample of Q in ethanol. Table 5 lists the values of the parameters for all samples. The IC_{50} value of the standard mixture was in agree with several found in the literature so it is concluded that the procedure was validated. It should be noted that the higher the antioxidant capacity, the lower the IC_{50} value. According this, the antioxidant capacity of the samples followed the sequence (Q in GOa) > (pure Q) > (Q in COa). This result indicates that G in Oa has a greater capacity to reduce the radical than C in Oa, which could be related to a slightly higher acidity of the linear alcohol. Finally, a time-course DPPH assay was performed for each sample, measuring the DPPH decay (A_s at λ=517 nm) from 2 to 60 min. For ascorbic acid, the reaction was virtually instantaneous. The results were very similar for Q in GOa and COa, reaching steady state later than for Q in ethanol (Fig. S5). A quantification of the reaction rate can be performed by differentiating the curves of the Fig. S5. At 10 min, the values for Q in ethanol, Q in GOa, and Q in COa were $2.5{\cdot}10^{-3}$, $7.5{\cdot}10^{-3}$, and $5.0{\cdot}10^{-3}$ min^{-1}, respectively. At 30 min, they were $0.5{\cdot}10^{-3}$, $1.5{\cdot}10^{-3}$, and $1.25{\cdot}10^{-3}$ min^{-1}, and 0, $0.5{\cdot}10^{-3}$, and $0.5{\cdot}10^{-3}$ min^{-1} at 60 min.

Table 5
Coefficients and regression of the (%In_{DPPH} − Q_s) linear relationships[a] and antioxidant capacity in terms of half maximal inhibitory concentration (IC_{50}).

	A	B/(mL/μg)	R^2	IC_{50}/(μg/mL)
Ascorbic acid[b]	13.995	16.736	0.994	2.15/2.08[c]/2.52[d]
Quercetin[b]	32.305	15.842	0.995	1.15/0.87[e]
Q in GOa[b]	45.623	5.915	0.985	0.74
Q in COa[b]	351.17	8.575	0.980	1.73

[a] Eq. (2).
[b] Ethanol was used as solvent.
[c] Ref. [72].
[d] Ref. [73].
[e] Ref. [74].

5. Conclusion

The temperatures and enthalpies of phase change and several thermophysical properties of the equimolar mixtures of oleic acid and geraniol or cinnamyl alcohol were measurement and discussed. The properties were density, speed of sound, refractive index, isobaric molar heat capacity, surface tension, and dynamic viscosity. They were determined from 283.15 K to 338.15 K and at a pressure of 0.1 MPa. In addition, different derived properties were calculated, correlations were applied, and the PC-SAFT EoS was validated for these systems. Finally, a study was conducted on the ability of both mixtures to dissolve quercetin, as well as the antioxidant capacity of the final ternary mixtures.

The thermophysical characterization indicated that the COa was more compact, structured, and viscous mixture than GOa. From an operational perspective, the densities were sufficiently lower than those of water to ensure proper separation in two-phase extraction processes. Furthermore, the slightly moderate viscosity values suggested proper mass transfer processes. A high linearity was obtained in the surface tension-refractive index, and surface tension-viscosity correlations. Also, the PC-SAFT EoS well predicted the density and molar isobaric heat capacity, with a mean relative deviation lower than 0.32% and 3.6%, respectively. These values indicated that this model adequately represented both systems under the conditions of this work. The critical temperatures obtained from different correlations and models were similar, which confirms the validity of these values. The results of the solubility tests indicated that Q was almost 10% more soluble in GOa than in COa. This fact could be related to the greater capacity of G compared to C to occupy the target space. Both mixtures showed a solvent capacity for Q much greater than water, up to $1.3{\cdot}10^3$-fold. The structure of Q would explain its greater affinity for more polarizable solvents. Regarding the antioxidant capacity of DPPH, the mixture with G presented a lower IC_{50} value compared to pure Q, and the mixture with C a slightly higher value.

CRediT authorship contribution statement

Ana Gavín: Resources, Investigation, Data curation. **Daniel Juan:** Methodology, Investigation, Data curation. **José Muñoz-Embid:** Validation, Formal analysis. **Mohammadreza Haftbaradaran Esfahani:** Methodology, Data curation. **Carlos Lafuente:** Writing – original draft, Project administration. **Manuela Artal:** Writing – review & editing, Project administration.

Declaration of competing interest

The authors declare that they have no known competing financial interests or personal relationships that could have influenced the work reported in this paper.

Acknowledgments

PLATON research group acknowledges financial support from Gobierno de Aragón and Fondo Social Europeo “Construyendo Europa desde Aragón” _E31_23R.

Appendix A. Supplementary data

Supplementary data to this article can be found online at https://doi.org/10.1016/j.molliq.2026.129573.

Data availability

The authors confirm that the data supporting the findings of this study are available within the article and its supplementary materials

References

[1] C.J. Clarke, W.C. Tu, O. Levers, A. Bröhl, J.P. Hallett, Green and sustainable solvents in chemical processes, Chem. Rev. 118 (2018) 747–800, https://doi.org/10.1021/acs.chemrev.7b00571.
[2] F. Guthrie, LII. *On eutexia*, Lond. Edinb. Dublin Philos. Mag. J. Sci. 17 (1884) 462–482, https://doi.org/10.1080/14786448408627543.
[3] A.P. Abbott, G. Capper, D.L. Davies, R.K. Rasheed, V. Tambyrajah, Novel solvent properties of choline chloride/urea mixtures, Chem. Commun. 9 (2003) 70–71, https://doi.org/10.1039/b210714g.
[4] D.O. Abranches, J.A.P. Coutinho, Everything you wanted to know about deep eutectic solvents but were afraid to be told, Annu. Rev. Chem. Biomol. Eng. 14 (2023) 141–163, https://doi.org/10.1146/annurev-chembioeng-101121-085323.
[5] J. Afonso, A. Mezzetta, I.M. Marrucho, L. Guazzelli, History repeats itself again: Will the mistakes of the past for ILs be repeated for DESs? From being considered ionic liquids to becoming their alternative: the unbalanced turn of deep eutectic solvents, Green Chem. 25 (2022) 59–105, https://doi.org/10.1039/d2gc03198a.
[6] M.A.R. Martins, S.P. Pinho, J.A.P. Coutinho, Insights into the nature of eutectic and deep eutectic mixtures, J. Solut. Chem. (2018), https://doi.org/10.1007/s10953-018-0793-1.
[7] D.O. Abranches, M.A.R. Martins, L.P. Silva, N. Schaeffer, S.P. Pinho, J.A. P. Coutinho, Phenolic hydrogen bond donors in the formation of non-ionic deep eutectic solvents: the quest for type v des, Chem. Commun. 55 (2019) 10253–10256, https://doi.org/10.1039/c9cc04846d.
[8] E. Chevé-Kools, Y.H. Choi, C. Roullier, G. Ruprich-Robert, R. Grougnet, F. Chapeland-Leclerc, F. Hollmann, Natural deep eutectic solvents (NaDES): green solvents for pharmaceutical applications and beyond, Green Chem. 27 (2025) 8360–8385, https://doi.org/10.1039/D4GC06386D.
[9] B.B. Hansen, S. Spittle, B. Chen, D. Poe, Y. Zhang, J.M. Klein, A. Horton, L. Adhikari, T. Zelovich, B.W. Doherty, B. Gurkan, E.J. Maginn, A. Ragauskas, M. Dadmun, T.A. Zawodzinski, G.A. Baker, M.E. Tuckerman, R.F. Savinell, J. R. Sangoro, Deep eutectic solvents: a review of fundamentals and applications, Chem. Rev. 121 (2021) 1232–1285, https://doi.org/10.1021/acs.chemrev.0c00385.
[10] F. Oyoun, A. Toncheva, L.C. Henríquez, R. Grougnet, F. Laoutid, N. Mignet, K. Alhareth, Y. Corvis, Deep eutectic solvents: an eco-friendly design for drug engineering, ChemSusChem 16 (2023), https://doi.org/10.1002/cssc.202300669.
[11] I.D. Boateng, Evaluating the status quo of deep eutectic solvent in food chemistry. Potentials and limitations, Food Chem. 406 (2023), https://doi.org/10.1016/j.foodchem.2022.135079.
[12] R. Alsaidi, T. Thiemann, Use of natural deep eutectic solvents (NADES) in food science and food processing, Sustainability 17 (2025) 2293, https://doi.org/10.3390/su17052293.
[13] M.J. Gidado, A.A.N. Gunny, I.M. AlNashef, Deep eutectic solvents as green alternatives in postharvest fruit preservation: a comprehensive review, Food Bioprocess Technol. (2025), https://doi.org/10.1007/s11947-025-04016-z.
[14] X. Yun, Y. Zhou, H. Shi, Z. Li, Y. Yun, M. Xie, L. Chen, Combination of plant essential oils and ice: extraction, encapsulation and applications in food preservation, Food Chem. 493 (2025) 145793, https://doi.org/10.1016/j.foodchem.2025.145793.
[15] Y. Li, Q. Liang, X. Jiang, Y. Zhang, W. Shi, Betaine-based natural deep eutectic solvents (NADESs) for enhanced cryoprotection: insights into hydrogen bonding behavior and antifreeze mechanisms, Food Chem. 493 (2025) 145893, https://doi.org/10.1016/j.foodchem.2025.145893.
[16] R. Castro-Muñoz, Advances in deep eutectic solvents as extracting media toward heavy metals from natural, processed and commercialized food products, Food Chem. 486 (2025) 144599, https://doi.org/10.1016/j.foodchem.2025.144599.
[17] Á. Luque-Uría, F. Pradanas González, F. Navarro-Villoslada, E. Benito-Peña, Natural deep eutectic solvents as a green alternative for extracting contaminants from food samples: a review, J. Anal. Test. (2025), https://doi.org/10.1007/s41664-025-00383-w.
[18] N. Zardo, C. Will, A.V. Santos, D. Galvan, E. Carasek, Exploring HDES as a sustainable green extractant phase in HF-MMLLE technique for assessment of PAHs in hot beverages and evaluation of potential dietary exposure risks for the brazilian population, Food Chem. 493 (2025) 145680, https://doi.org/10.1016/j.foodchem.2025.145680.
[19] D. Artigas-Hernández, A. Berzosa, D. Aguilar-Machado, J. Raso, M. Artal, Using eutectic solvents for extracting astaxanthin from dry biomass of xanthophyllomyces dendrorhous pretreated by pulsed electric fields, Sep. Purif. Technol. 324 (2023), https://doi.org/10.1016/j.seppur.2023.124496.
[20] S. Ma, C. Cai, Q. Lu, Z. Tan, A review of green solvents for the extraction and separation of bioactive ingredients from natural products, Food Chem. 478 (2025) 143703, https://doi.org/10.1016/j.foodchem.2025.143703.
[21] J. Marañés, A. Berzosa, F. Bergua, J. Marín-Sánchez, J. Raso, M. Artal, Eutectic mixtures based on oleic acid and pulsed electric fields: a strategy for the extraction of astaxanthin from dry biomass of xanthophyllomyces dendrorhous, Foods 14 (2025) 2371, https://doi.org/10.3390/foods14132371.
[22] J. Osamede Airouyuwa, N. Sivapragasam, A. Ali Redha, S. Maqsood, Sustainable green extraction of anthocyanins and carotenoids using deep eutectic solvents (DES): a review of recent developments, Food Chem. 448 (2024) 139061, https://doi.org/10.1016/j.foodchem.2024.139061.
[23] M.H. Esfahani, F. Bergua, I. Delso, C. Lafuente, M. Artal, Geraniol: L-menthol eutectic mixtures; thermophysical properties and drug solubility, Sustain. Chem. Pharm. 46 (2025) 102070, https://doi.org/10.1016/j.scp.2025.102070.
[24] C. Wennberg, M. Lundborg, E. Lindahl, L. Norlén, Understanding drug skin permeation enhancers using molecular dynamics simulations, J. Chem. Inf. Model. 63 (2023) 4900–4911, https://doi.org/10.1021/acs.jcim.3c00625.
[25] P. Harten, T. Martin, M. Gonzalez, D. Young, The software tool to find greener solvent replacements, PARIS III, Environ. Prog. Sustain. Energ. 39 (2020) 1–7, https://doi.org/10.1002/ep.13331.
[26] H. Sels, H. De Smet, J. Geuens, SUSSOL-using artificial intelligence for greener solvent selection and substitution, Molecules 25 (2020) 1–26, https://doi.org/10.3390/molecules25133037.
[27] S. Singh, A. Mishra, Alka, unlocking the therapeutic potential of geraniol: an alternative perspective for metabolic disease management, Inflammopharmacology 32 (2024) 3653–3668, https://doi.org/10.1007/s10787-024-01582-0.
[28] N. Viswanadh, P. Mujumdar, M. Sasikumar, S.S. Kunte, M. Muthukrishnan, An alternate synthesis of appetite suppressant (r)-2-benzylmorpholine employing sharpless asymmetric epoxidation strategy, Tetrahedron Lett. 57 (2016) 861–863, https://doi.org/10.1016/j.tetlet.2016.01.032.
[29] PubChem Database. https://pubchem.ncbi.nlm.nih.gov/, 2026.
[30] L. Zou, C. Li, X. Chen, F. Yu, Q. Huang, L. Chen, W. Wu, Q. Liu, The anti-inflammatory effects of cinnamyl alcohol on sepsis-induced mice via the NLRP3 inflammasome pathway, Ann. Transl. Med. 10 (2022) 48–58, https://doi.org/10.21037/atm-21-6130.
[31] Y. Wang, H. Shi, L. Chen, T. Su, X. Luo, X. Xie, H. Ji, Z. Qin, 2D vanadium carbide (V2CTx) MXene supported NiIn intermetallic compounds for the selective hydrogenation of cinnamaldehyde to cinnamyl alcohol, reaction kinetics, mechanisms and catalysis, 2025, https://doi.org/10.1007/s11144-025-02866-4.
[32] Y. Wang, J. Jin, G. Wu, W. Wei, Q. Jin, X. Wang, Omega-9 monounsaturated fatty acids: a review of current scientific evidence of sources, metabolism, benefits, recommended intake, and edible safety, Crit. Rev. Food Sci. Nutr. (2024), https://doi.org/10.1080/10408398.2024.2313181.
[33] M. Vlacha, A. Giannakas, P. Katapodis, H. Stamatis, A. Ladavos, N.M. Barkoula, On the efficiency of oleic acid as plasticizer of chitosan/clay nanocomposites and its role on thermo-mechanical, barrier and antimicrobial properties - comparison with glycerol, Food Hydrocoll. 57 (2016) 10–19, https://doi.org/10.1016/j.foodhyd.2016.01.003.
[34] R. Pastor, C. Bouzas, J.A. Tur, Beneficial effects of dietary supplementation with olive oil, oleic acid, or hydroxytyrosol in metabolic syndrome: systematic review and meta-analysis, Free Radic. Biol. Med. 172 (2021) 372–385, https://doi.org/10.1016/j.freeradbiomed.2021.06.017.
[35] Oleic Acid Market Forecast and Outlook (2025–2035). Https://Www.Futuremarketinsights.Com/Reports/Oleic-Acid-Market, 2025.
[36] A. Mohan, G. Dummi Mahadevan, V. Anand Iyer, T.K. Mukherjee, V. Haribhai Patel, R. Kumar, N. Siddiqui, M. Nayak, P.K. Maurya, P. Kumar, Dietary flavonoids in health and diseases: a concise review of their role in homeostasis and therapeutics, Food Chem. 487 (2025) 144674, https://doi.org/10.1016/j.foodchem.2025.144674.
[37] I.G. Osojnik Črnivec, M. Skrt, T. Polak, D. Šeremet, P. Mrak, D. Komes, U. Vrhovšek, N. Poklar Ulrih, Aspects of quercetin stability and its liposomal enhancement in yellow onion skin extracts, Food Chem. 459 (2024) 140347, https://doi.org/10.1016/j.foodchem.2024.140347.
[38] L. Jaganmohanrao, Valorization of onion wastes and by-products using deep eutectic solvents as alternate green technology solvents for isolation of bioactive phytochemicals, Food Res. Int. 206 (2025) 115980, https://doi.org/10.1016/j.foodres.2025.115980.
[39] W. Pitacco, C. Samorì, L. Pezzolesi, V. Gori, A. Grillo, M. Tiecco, M. Vagnoni, P. Galletti, Extraction of astaxanthin from haematococcus pluvialis with hydrophobic deep eutectic solvents based on oleic acid, Food Chem. 379 (2022), https://doi.org/10.1016/j.foodchem.2022.132156.

[40] S. Anjali, Pandey, density and dynamic viscosity of Hydrotrope-assisted surfactant free microemulsions formed with hydrophobic deep eutectic solvents, J. Chem. Eng. Data 69 (2024) 3718–3729, https://doi.org/10.1021/acs.jced.4c00182.
[41] Z. Jiang, X. Wang, H. Deng, W. Zhang, Y. Zhao, J. Zhao, Y. Li, Study of the experimental and microscopic mechanism of the removal of phenolic compounds from wastewater based on hydrophobic deep eutectic solvents, J. Mol. Liq. 406 (2024) 125055, https://doi.org/10.1016/j.molliq.2024.125055.
[42] E. Baka, Development and Examination of Solubility Measurement Methods for Drug Solubility Determination, Smmelweis University, Budapest, 2010.
[43] M.S. Blois, Antioxidant determinations by the use of a stable free radical, Nature 181 (1958) 1199–1200, https://doi.org/10.1038/1811199a0.
[44] J. Gross, G. Sadowski, Perturbed-chain SAFT: an equation of state based on a perturbation theory for chain molecules, Ind. Eng. Chem. Res. 40 (2001) 1244–1260, https://doi.org/10.1021/ie0003887.
[45] J. Gross, G. Sadowski, Application of the perturbed-chain SAFT equation of state to associating systems, Ind. Eng. Chem. Res. 41 (2002) 5510–5515, https://doi.org/10.1021/ie010954d.
[46] P.R.S. dos Santos, F.A.P. Voll, L.P. Ramos, M.L. Corazza, Esterification of fatty acids with supercritical ethanol in a continuous tubular reactor, J. Supercrit. Fluids 126 (2017) 25–36, https://doi.org/10.1016/j.supflu.2017.03.002.
[47] M.H. Esfahani, F. Bergua, I. Delso, C. Lafuente, M. Artal, Geraniol and hydrophobic geraniol: thymol eutectic mixtures: structure and thermophysical characterization, Ind. Crop. Prod. 222 (2024) 119781, https://doi.org/10.1016/j.indcrop.2024.119781.
[48] M. Taherzadeh, R. Haghbakhsh, A.R.C. Duarte, S. Raeissi, Estimation of the heat capacities of deep eutectic solvents, J. Mol. Liq. 307 (2020) 112940, https://doi.org/10.1016/j.molliq.2020.112940.
[49] E.A. Guggenheim, The principle of corresponding states, J. Phys. Chem. 13 (1945) 253–261.
[50] J.L.L. Shereshefsky, Surface tension of saturated vapors and the equation of eötvos, J. Phys. Chem. 35 (1930) 1712–1720, https://doi.org/10.1021/j150324a014.
[51] H.A. Papazian, Correlation of surface tension between various liquids, J. Am. Chem. Soc. 93 (1971) 5634–5636, https://doi.org/10.1021/ja00751a008.
[52] A.H. Pelofsky, Surface tension-viscosity relation for liquids, J. Chem. Eng. Data 11 (1966) 394–397, https://doi.org/10.1021/je60030a031.
[53] L.A. García-Zapateiro, J.M. Franco, C. Valencia, M.A. Delgado, C. Gallegos, Viscous, thermal and tribological characterization of oleic and ricinoleic acids-derived estolides and their blends with vegetable oils, J. Ind. Eng. Chem. 19 (2013) 1289–1298, https://doi.org/10.1016/j.jiec.2012.12.030.
[54] P. Tandon, G. Förster, R. Neubert, S. Wartewig, Phase transitions in oleic acid as studied by x-ray diffraction and FT-Raman spectroscopy, J. Mol. Struct. 524 (2000) 201–215, https://doi.org/10.1016/S0022-2860(00)00378-1.
[55] V. Štejfa, F. Dergal, I. Mokbel, M. Fulem, J. Jose, K. Růžička, Vapor pressures and thermophysical properties of selected monoterpenoids, Fluid Phase Equilib. 406 (2015) 124–133, https://doi.org/10.1016/j.fluid.2015.07.031.
[56] E. Pérez-Pueyo, H. Artigas, M.H. Esfahani, C. Lafuente, M. Artal, Thermophysical properties of eutectic mixtures composed by oleic acid and components of essential oils, Food Res. Int. (2025) 117802, https://doi.org/10.1016/j.foodres.2025.117802.
[57] B. Jacobson, Ultrasonic velocity in liquids and liquid mixtures, J. Chem. Phys. 20 (1952) 927–928, https://doi.org/10.1063/1.1700615.
[58] I.M. Aroso, A. Paiva, R.L. Reis, A.R.C. Duarte, Natural deep eutectic solvents from choline chloride and betaine – physicochemical properties, J. Mol. Liq. 241 (2017) 654–661, https://doi.org/10.1016/j.molliq.2017.06.051.
[59] D.J.G.P. Van Osch, C.H.J.T. Dietz, J. Van Spronsen, M.C. Kroon, F. Gallucci, M. Van Sint Annaland, R. Tuinier, A search for natural hydrophobic deep eutectic solvents based on natural components, ACS Sustain. Chem. Eng. 7 (2019) 2933–2942, https://doi.org/10.1021/acssuschemeng.8b03520.
[60] L.S. Garca-Coln, L.F. del Castillo, P. Goldstein, Theoretical basis for the Vogel-Fulcher-Tammann equation, Phys. Rev. B 40 (1989) 7040–7044, https://doi.org/10.1103/PhysRevB.40.7040.
[61] F. Bergua, M. Castro, J. Muñoz-Embid, C. Lafuente, M. Artal, Hydrophobic eutectic solvents: Thermophysical study and application in removal of pharmaceutical products from water, Chem. Eng. J. 411 (2021), https://doi.org/10.1016/j.cej.2021.128472.
[62] F. Bergua, I. Delso, J. Muñoz-Embid, C. Lafuente, M. Artal, Structure and properties of two glucose-based deep eutectic systems, Food Chem. 336 (2021) 127717, https://doi.org/10.1016/j.foodchem.2020.127717.
[63] F. Bergua, M. Castro, C. Lafuente, M. Artal, Thymol+l-menthol eutectic mixtures: Thermophysical properties and possible applications as decontaminants, J. Mol. Liq. 368 (2022) 120789, https://doi.org/10.1016/j.molliq.2022.120789.
[64] F. Bergua, M. Castro, J. Muñoz-Embid, C. Lafuente, M. Artal, L-menthol-based eutectic solvents: characterization and application in the removal of drugs from water, J. Mol. Liq. 352 (2022) 118754, https://doi.org/10.1016/j.molliq.2022.118754.
[65] N. López, I. Delso, D. Matute, C. Lafuente, M. Artal, Characterization of xylitol or citric acid: choline chloride: water mixtures: structure, thermophysical properties, and quercetin solubility, Food Chem. 306 (2020), https://doi.org/10.1016/j.foodchem.2019.125610.
[66] G. Oliveira, J.P. Wojeicchowski, F.O. Farias, L. Igarashi-Mafra, R. de Pelegrini Soares, M.R. Mafra, Enhancement of biomolecules solubility in aqueous media using designer solvents as additives: an experimental and COSMO-based models' approach, J. Mol. Liq. 318 (2020) 114266, https://doi.org/10.1016/j.molliq.2020.114266.
[67] E. Rodríguez-Juan, S. López, R. Abia, F.J.G. Muriana, J. Fernández-Bolaños, A. García-Borrego, Antimicrobial activity on phytopathogenic bacteria and yeast, cytotoxicity and solubilizing capacity of deep eutectic solvents, J. Mol. Liq. 337 (2021) 116343, https://doi.org/10.1016/j.molliq.2021.116343.
[68] V. Suryanti, F.R. Wibowo, S. Khotijah, N. Andalucki, Antioxidant activities of cinnamaldehyde derivatives, IOP Conf. Ser.: Mater. Sci. Eng. 333 (2018) 012077, https://doi.org/10.1088/1757-899X/333/1/012077.
[69] M.C. Foti, Use and abuse of the DPPH • radical, J. Agric. Food Chem. 63 (2015) 8765–8776, https://doi.org/10.1021/acs.jafc.5b03839.
[70] S.B. Kedare, R.P. Singh, Genesis and development of DPPH method of antioxidant assay, J. Food Sci. Technol. 48 (2011) 412–422, https://doi.org/10.1007/s13197-011-0251-1.
[71] K. Mishra, H. Ojha, N.K. Chaudhury, Estimation of antiradical properties of antioxidants using DPPH- assay: a critical review and results, Food Chem. 130 (2012) 1036–1043, https://doi.org/10.1016/j.foodchem.2011.07.127.
[72] F. Abderrahim, S.M. Arribas, M.C. Gonzalez, L. Condezo-Hoyos, Rapid high-throughput assay to assess scavenging capacity index using DPPH, Food Chem. 141 (2013) 788–794, https://doi.org/10.1016/j.foodchem.2013.04.055.
[73] O.P. Sharma, T.K. Bhat, DPPH antioxidant assay revisited, Food Chem. 113 (2009) 1202–1205, https://doi.org/10.1016/j.foodchem.2008.08.008.
[74] G. Morales, A. Paredes, P. Sierra, L.A. Loyola, Antioxidant activity of 50% aqueous - ethanol extract from acantholippia deserticola, Biol. Res. 41 (2008), https://doi.org/10.4067/S0716-97602008000200004.